Land Cover Classification from Hyperspectral Images Using Regularized Hybrid CNN and ADAM

Yetti Yuniati[1*] and Ezra Taufiqurrahman[1]

[1]*Departement of Electrical Engineering, Universitas Lampung*

Jl. Prof. Dr. Soemantri Brojonegoro No. 1 Gedong Meneng, Bandar Lampung 35144, Indonesia

[*]*Coresponding author, Email: yetti.yuniati@eng.unila.ac.id*

Abstract— The utilization of hyperspectral imagery offers enhanced detail and accuracy for environmental monitoring and natural resource management, particularly through land cover classification. Hyperspectral data capture spectral signatures across numerous wavelengths, allowing precise differentiation of various surface materials and land types. While numerous approaches have been proposed for hyperspectral image classification, many suffer from overly complex model structures and suboptimal performance, limiting their practical application. This study introduces a simplified yet effective architecture by implementing a Regularized Hybrid Convolutional Neural Network (CNN) optimized using Adaptive Moment Estimation (ADAM). The proposed model is evaluated on the widely used Pavia Center hyperspectral dataset to assess its performance in land cover classification tasks. The model achieves a notable Overall Accuracy of 99.25% and Average Accuracy of 97.50%, demonstrating its capability in handling high-dimensional hyperspectral data with reduced model complexity. Additionally, a comparative analysis with conventional CNN architectures is conducted, highlighting the superior performance and efficiency of the proposed approach. These findings underscore the potential of regularized hybrid CNNs as a reliable and scalable solution for hyperspectral image classification, especially in applications requiring high precision and reduced computational overhead.

Keywords— ADAM; Classification ; Hyperspectral imagery; Hybrid CNN; Land cover.

I. INTRODUCTION

The development of an area can result in physical changes caused by either human or natural factors. To understand surface phenomena and as a basis for land-based management planning, accurate information about land cover is essential. Conventional land monitoring methods, such as field surveys, are often time-consuming, costly, and unable to provide detailed and comprehensive information. In response to these limitations, remote sensing technology has been used to monitor land cover. However, some studies indicate that conventional remote sensing still has limitations in spatial and spectral resolution, which can reduce the accuracy of the obtained information.

The development of an area can result in physical changes caused by either human or natural factors. To understand surface phenomena and as a basis for land-based management planning, accurate information about land cover is essential. Conventional land monitoring methods, such as field surveys, are often time-consuming, costly, and unable to provide detailed and comprehensive information [1]. In response to these limitations, remote sensing technology has been used to monitor land cover. However, some studies indicate that conventional remote sensing still has limitations in spatial and spectral resolution, which can reduce the accuracy of the obtained information.

Remote sensing is a technology that utilizes sensors or instruments on aircraft or satellites to collect information about the environment, such as satellite imagery or electromagnetic spectra. One highly accurate type of remote sensing data is hyperspectral imagery, which can provide very detailed information about the Earth's surface [2]. Hyperspectral remote sensing technology offers a solution by providing very high spectral resolution, allowing for more detailed identification and analysis of various land cover types.

Previous research has shown that hyperspectral remote sensing can identify land characteristics more accurately compared to other technologies [3]. However, the use of this technology is still limited, especially in practical applications for land planning and management. Therefore, this research aims to address this gap by exploring and implementing hyperspectral remote sensing technology for more detailed and accurate land cover monitoring. By utilizing more than 100 different wavelength bands, this technology can produce highly comprehensive information about land conditions [4]. This has significantly contributed to improving the efficiency and effectiveness of land planning and management, as well as provide a more solid database for land use decision-making.

The primary motivation for this research is to overcome the limitations of conventional remote sensing technology in land cover monitoring. By implementing hyperspectral remote sensing technology, which offers very high spectral resolution, this study aims to provide a more innovative and effective solution for land cover monitoring and management [5].

This research implements hyperspectral remote sensing technology to obtain more detailed and accurate information

Received 20 June 2024, Revised 19 June 2025, Accepted 22 June 2025.

DOI: https://doi.org/10.15294/jte.v16i1.7732

about land cover, which can be used as a basis for land planning and management. The use of hyperspectral imagery, utilizing more than 100 different wavelength bands, results in highly comprehensive data [6]. In hyperspectral imagery, each electromagnetic spectrum is organized in the form of a stack of two-dimensional images, forming a data cube consisting of various layers. Each layer represents a spectral band with different wavelengths, allowing for a more detailed analysis of various land cover types [7].

The main contribution of this research is the development of an optimized Convolutional Neural Network (CNN) framework tailored for hyperspectral land cover images in the Pavia Center dataset. This framework compares the performance of the Regularized Hybrid CNN method with conventional CNN methods in classifying hyperspectral land cover images in the same dataset [8]. The Regularized Hybrid CNN method combines 3D and 2D CNN techniques to maximize the utilization of two features in hyperspectral images, utilizing both spatial and spectral correlations simultaneously, thus extracting more discriminative features and improving class specificity, achieving better accuracy [9].

Optimization in this study compares optimization methods using Stochastic Gradient Descent (SGD) and Adaptive Moment Estimation (ADAM), showing that ADAM optimization performs better. Additionally, this study implements dropout regularization techniques to prevent overfitting by randomly eliminating neurons during the forward and backward pass phases and applying Ridge Regularization to enhance model generalization in hyperspectral image classification [10].

II. METHODS

This study adopts a structured machine learning workflow that includes five main phases: problem definition, data preprocessing, model development, training and optimization, and performance evaluation. The objective is to enhance hyperspectral image classification using a hybrid deep learning model [11].

The process begins with clearly defining the research problem, which focuses on improving classification accuracy for land cover types using hyperspectral data. The Pavia Center dataset, comprising 1096×1096 pixels with 102 spectral bands and 9 land cover classes, was selected as the benchmark for model evaluation due to its rich spectral and spatial information. In the data preprocessing stage, raw hyperspectral data was first cleaned by eliminating spectral bands with low signal-to-noise ratios. To address class imbalance, oversampling techniques were applied, followed by data augmentation to enhance model generalization. The reflectance values were normalized to ensure consistent feature scaling across all input data. For model development, three types of Convolutional Neural Network (CNN) architectures were designed: a standard 2D CNN to capture spatial features, a 3D CNN to capture spectral-spatial relationships, and a Hybrid CNN that combines both. The proposed architecture, a Regularized Hybrid CNN, leverages the strengths of both 2D and 3D layers to improve classification accuracy. To mitigate overfitting, dropout layers and L2 regularization were integrated into the model. During the training phase, two optimization strategies Stochastic Gradient Descent (SGD) and Adam were compared. The ADAM optimizer was selected based on its stable convergence and higher accuracy throughout the training process.

Finally, model performance was evaluated using multiple metrics: Overall Accuracy (OA), Average Accuracy (AA), and Standard Deviation (SD) to assess variability. Additionally, a confusion matrix and class-wise classification report, including precision, recall, and F1-score [12], were used to analyze detailed performance. A summary of this workflow is illustrated in Figure 1 to provide a clear and structured overview of the entire research process.

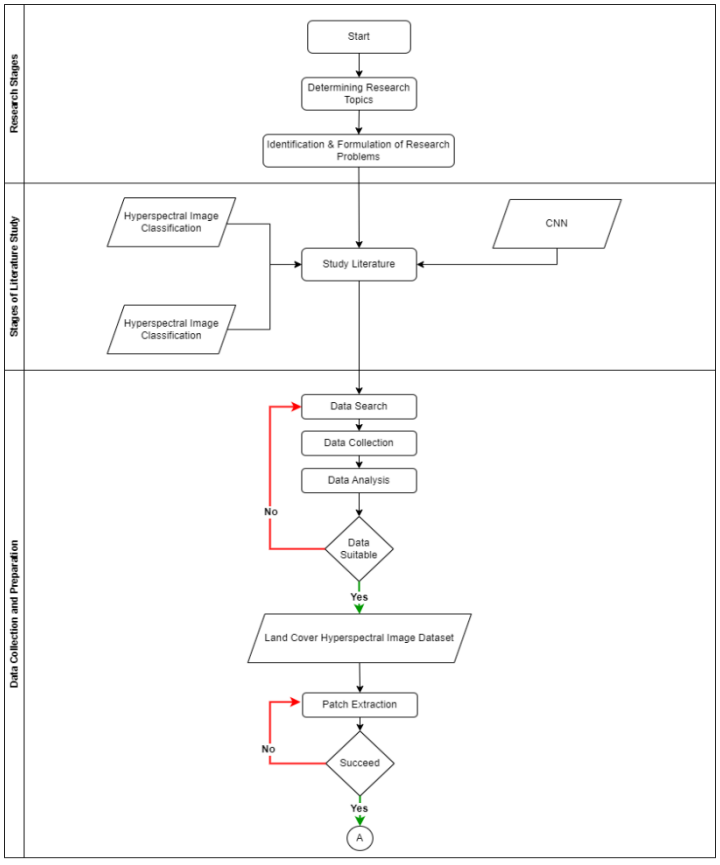

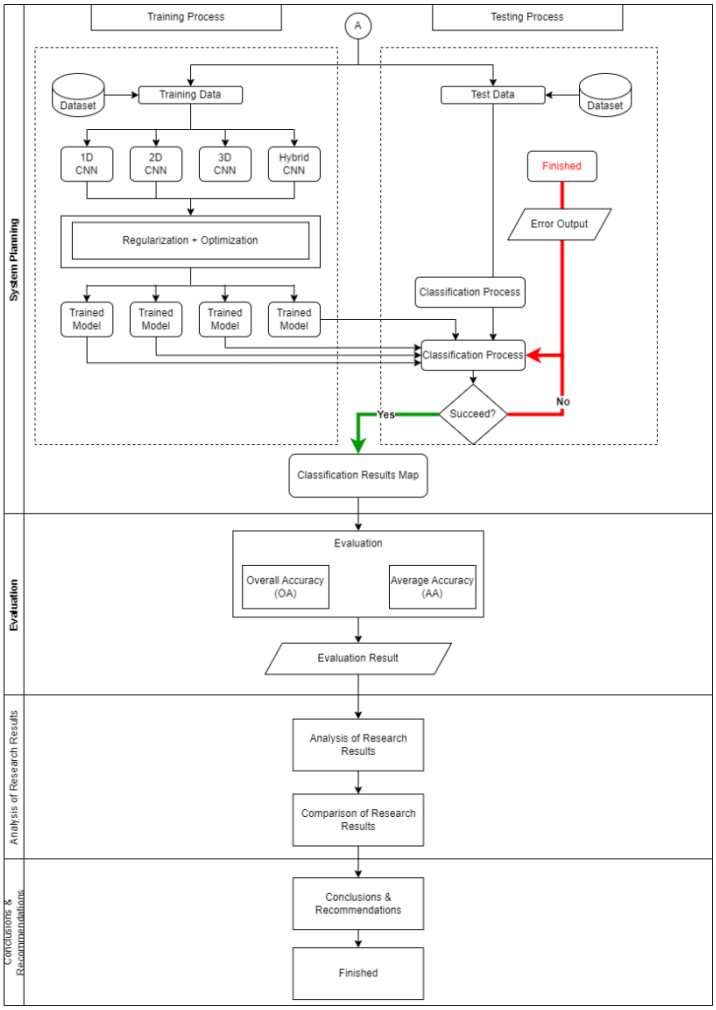

Figure 1. Research Flowchart

A. Data Analysis

The dataset utilized is the Pavia Center (PC) dataset. Band removal, involving the elimination of spectral bands considered to have low sensitivity, has been performed on each image within the dataset. The image size of Pavia Center (PC) is 1096 x 1096 with Band Spectral of 102 and Spasial Resolution is 1,3.

The class dataset of the Pavia Center (PC) Table 3.4, which is the Pavia Center (PC) Class Dataset Table, provides highly relevant information regarding the composition and characteristics of classes within the Pavia Center dataset. In this dataset, there are 9 different classes, with each class having a detailed number of samples as listed in the table.

Figure 2 displays false color and ground truth (truth map) as references for classifying the data classes.

(a) (b)

Figure 2. (a) False Color; (b) Groundtruth Dataset PC

Visualization of PC Data in figure 3, in Several Hyperspectral Bands, presents an example visualization of hyperspectral data from the Pavia Center (PC) dataset in a number of randomly selected bands. This visualization provides a crucial visual representation of the nature and characteristics of the hyperspectral data used in this research. By examining various bands randomly, researchers can identify patterns, features, and variations present in the data.

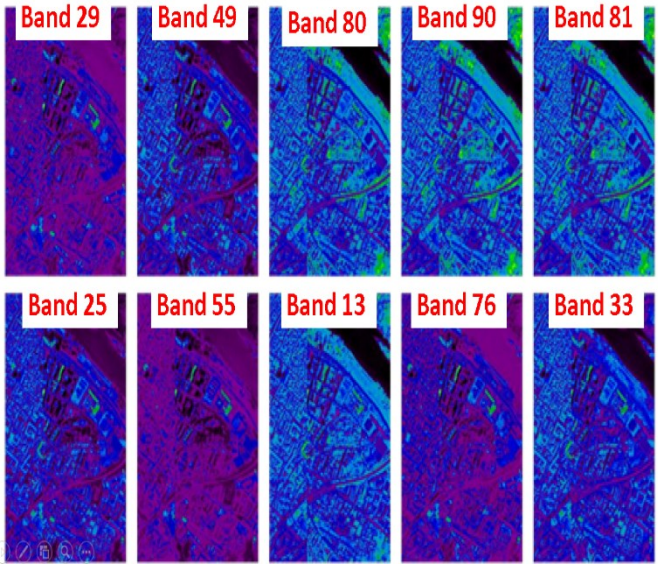

Figure 3. Data PC Visualization

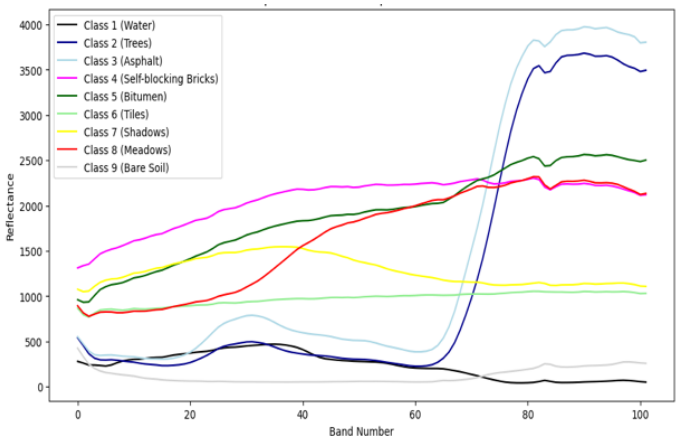

Figure 4. Average Reflectance Spectrum of Each Class in the Pavia Dataset

In hyperspectral image analysis, the mean spectrum reflectance refers to the average reflectance values across various spectral bands reflecting the spectral characteristics of different objects or materials in the image [13]. This is performed by taking hyperspectral images from the Pavia dataset, which contain reflectance information across multiple spectral bands. In the context of this research, specific wavelength information for each band is not available, thus precise wavelength analysis cannot be conducted, and the reflectance units used in the output code are numerical units representing the intensity of light reflected by materials in the hyperspectral image. This is because the dataset does not provide information indicating reflectance units explicitly. However, in hyperspectral images, reflectance is often measured in units such as digital numbers (DN) or "count." These values reflect the light intensity detected by the hyperspectral sensor across various spectral bands.

The average spectrum is displayed in Figure 4, Average Reflectance Spectrum of Each Class in the Pavia Dataset. In Figure 4, the Mean spectrum illustrates the average spectral response or reflectance level for each class in the hyperspectral image. In the example provided, the difference between class 8 and class 9 is evident in their average spectral characteristics. Class 8 exhibits reflectance levels that tend to be higher (ranging from 1000 to 2000 reflectance) compared to class 9, which has lower reflectance levels (ranging from 300 to 500 reflectance) across various spectral bands. This difference reflects the distinct spectral properties between the two classes, enabling the identification of the types of materials or objects present in the hyperspectral image based on their spectral characteristics.

The process of calculating the mean spectrum is carried out by grouping data based on different classes within the image, which are identified by the ground truth labels (Pavia_gt.mat). The average reflectance spectrum is computed for each class by taking the average reflectance values across each spectral band. This creates average spectra reflecting the average spectral response for materials within that class [14]. Although specific wavelength information is not available, the mean spectrum can still be considered as a means to distinguish spectral characteristics between different classes in the hyperspectral image [15][16].

In the context of this research on hyperspectral image analysis using the Pavia Center dataset, the data used is already in the form of numerical spectral data in a numeric format (.mat), hence there is no explicitly available wavelength information for each spectral band in this dataset. The lack of wavelength information may pose a challenge when attempting to determine where each band lies in the electromagnetic spectrum, such as NIR, IR, or MIR categories. Despite the absence of specific wavelength information, this analysis can still provide useful insights in identifying materials and components in the hyperspectral image. This is relevant in the context of this research, which aims to classify and identify various object classes based on their average spectral responses [17].

B. Classification Process

At this stage, spectral and spatial information from the hyperspectral image map is extracted using the predefined model. Several testing experiments will be conducted with combinations of the Regularized Hybrid CNN method with Adaptive Moment Estimation (Adam) optimization and other conventional CNN methods [18].

The first step in the hyperspectral image classification process for land cover is preprocessing. Firstly, oversampling technique is implemented to duplicate data with low-label count. Secondly, the images will be enhanced with oversampling method then data augmentation will be performed to improve feature representation [19]. The classification process will be conducted using the standard 2D CNN method, 3D CNN method, and Regularized Hybrid CNN method. The classification results of these methods will be evaluated using several evaluation metrics and compared to analyze the performance of the methods used.

The classification process in this research in Figure 5 encompasses data processing involving several preprocessing stages as described earlier. The next stage involves feature extraction by predetermined layers. Finally, the extracted data is classified using fully connected layers.

C. Evaluation

Evaluation is conducted to measure the performance of the implemented algorithms on the land cover dataset. Three evaluation methods are used for comparing the performance of these algorithms: Overall Accuracy (OA), Average Accuracy (AA), and Variability Test with standard deviation, which processes the classification results by calculating data from the Confusion Matrix [19].

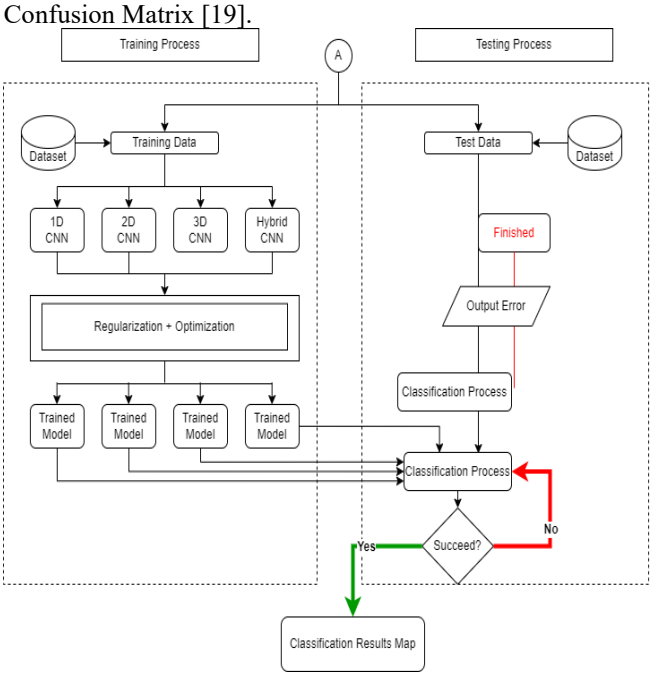

Figure 5. Classification Process

Overall Accuracy (OA) is measured using the following equation:

$$Overall\ acccuracy = \frac{(\text{number of correctly classified pixels})}{(total\ number\ of\ rest\ pixels)} \quad (1)$$

In this equation, "Number of correctly classified pixels" refers to the number of pixels accurately classified by the algorithm, and "Total number of pixels" represents the total number of pixels in the dataset.

Average Accuracy (AA) is calculated using the following equation:

$$Average\ acccuracy = \frac{(\text{number of accuracy for each class})}{(number\ of\ class)} \quad (2)$$

In this equation, the "Sum of accuracy for each class" represents the total accuracy of each class, and the "Number of classes" is the total number of classes in the classification task.

The variability test is measured using the standard deviation, calculated with the following equation:

$$\sigma = \sqrt{\frac{\Sigma(Xi-\mu)2}{N}} \quad (3)$$

Here, σ is the standard deviation, Xi represents individual values in the dataset, μ is the mean of those values, and N is the total number of values in the dataset. This equation is used to assess the variability of the classification results obtained from the applied algorithm.

III. Results and Discussion

In this study, we evaluated the performance of 14 different models, including 1D CNN, 2D CNN, 2D CNN with Regularization, 3D CNN, 3D CNN with Regularization, Hybrid CNN, and Hybrid CNN with Regularization. These models were tested using two optimization methods: Adam and SGD, on the Pavia Center dataset. Model evaluation was conducted using two metrics: Overall Accuracy (OA) and Average Accuracy (AA), along with standard deviation analysis to assess result variability. Table 1 presents a comparison of the performance of the tested models:

The results indicate that the Hybrid CNN with Regularization and Adam optimization (Models 13 and 14) provided higher Overall Accuracy (OA) and Average Accuracy (AA) compared to the other models. The detailed results can be seen in Table I. This model demonstrated a significant improvement in classification capability over basic models such as 1D CNN and 2D CNN. For instance, the Hybrid CNN with Regularization using Adam optimization achieved an OA of X% and an AA of Y%, whereas the 1D CNN with SGD only reached an OA of A% and an AA of B%.

The improved performance of the Hybrid CNN with Regularization compared to other models highlights that the combination of 2D and 3D CNN techniques with additional regularization effectively captures spatial and spectral features. These results are consistent with previous studies indicating that hybrid approaches can overcome the limitations of single CNN methods. Additionally, the application of Adam optimization showed better results than SGD, aligning with research that demonstrates Adam's advantages in faster convergence and stability.

TABLE I. Models Comparation

Model	Methods	*Optimizer*
1	1D CNN	SGD
2	1D CNN	Adam
3	2D CNN	SGD
4	2D CNN	Adam
5	Regularization + 2D CNN	SGD
6	Regularization + 2D CNN	Adam
7	3D CNN	SGD
8	3D CNN	Adam
9	Regularization + 3D CNN	SGD
10	Regularization + 3D CNN	Adam
11	*Hybrid* CNN	SGD
12	*Hybrid* CNN	Adam
13	Regularization + *Hybrid* CNN	SGD
14	Regularization + *Hybrid* CNN	Adam

A. Model Testing Results

The testing results of Model 14 represent the outcome of experiments conducted by applying a data processing approach using Hybrid CNN with Adam optimization method and with regularization technique on the Pavia dataset. In terms of accuracy, this model successfully achieved an Average Accuracy (AA) of 97.50%, indicating the average success rate in classifying various classes within the dataset. Additionally, the Overall Accuracy (OA) of the model reached 99.25%, providing an overview of how well the model was able to classify the entire dataset correctly. The results of this experiment are then presented in Table 3, which refers to the calculations of equations (1) and (3).

TABLE II. Accuration Result of Model 14

Class of Pavia	Accurations (%)
1	100%
2	99,68%
3	87,60%
4	97,36%
5	97,51%
6	96,45%
7	98,90%
8	99,98%
9	100%

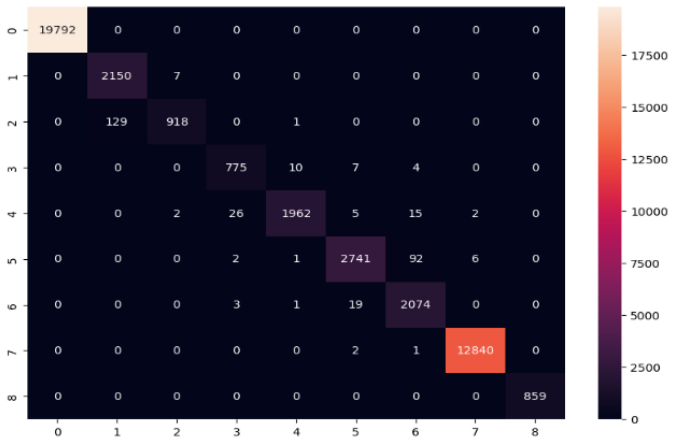

Figure 6. Confussion Matrix of Model 14

TABLE III. CLASSIFICATION REPORT OF MODEL 14

Class	Precision	Recall	F1-Score
1	1.00	1.00	1.00
2	0.94	1.00	0.97
3	0.99	0.88	0.93
4	0.96	0.97	0.97
5	0.99	0.98	0.98
6	0.99	0.96	0.97
7	0.95	0.99	0.97
8	1.00	1.00	1.00
9	1.00	1.00	1.00

Figure 6 shows the evaluation results of the Confusion Matrix for Model 14. Figure 6 shows the classes successfully classified by Model 14 on the Pavia dataset. It can be observed that the main diagonal in this Confusion Matrix tends to have high numbers, indicating many samples classified correctly. On the other hand, there are still numbers outside the main diagonal (prediction errors), which are generally low, but there are some with relatively high numbers of incorrect predictions.

The results of the Classification Report to provide detailed information about the performance of the classification model on various evaluation metrics, particularly in the context of multiclass, are shown in Table 4 of the Classification Report. The Classification Report results indicate that this model exhibits strong performance in classifying samples from various classes in the dataset. Based on the data above, Model 14 demonstrates excellent ability in classifying classes 1, 2, 4, 5, 6, 7, 8, and 9, with Precision, Recall, and F1-Score values reaching or approaching 1.00. This indicates that the model consistently and accurately identifies samples within these classes.

Based on the validity test results calculated according to equation (3). the resulting standard deviation is 0.0152. This is considered as an excellent indication in the analysis of data validity. in Figure 7. With such a low standard deviation value. the data spread becomes minimal. and a high level of consistency can be achieved. This indicates that the obtained results hardly deviate from the average during a series of measurements or observations.

In managing and understanding the training process to assess the effectiveness of the model used. it's essential to have timestamp information for each iteration conducted [20]. Below are the results of the timestamp for each iteration. displayed in Figure 8. This timestamp provides information about the time taken at each iteration stage. allowing for monitoring the model's progress over time and providing insights into potential performance improvements and resource savings [20].

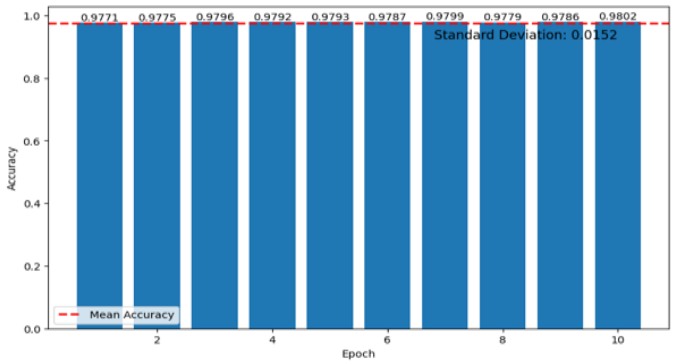

Figure 7. Validity Test of Standard Deviation for Model 14

The timestamp results from each training iteration displayed in Figure 8 serve as a crucial foundation for this research. providing a detailed understanding of the dynamics of model training. aiding in evaluating and optimizing the training process. and offering a robust framework for further analysis related to the efficiency and effectiveness of the model used.

Based on the image and timestamps recorded for each epoch. it can be concluded that within the sequence of 30 iterations conducted during model training. the time required to complete all iterations (steps) of batches within one epoch is approximately 5.68 minutes. From this information. it can be inferred that the model exhibits stability in the training duration across its epochs. This may indicate that the model has achieved good convergence and does not experience extreme fluctuations in training time.

Based on its classes. the output of this model will display a representative visualization of the identified area. Each color in the image represents a specific class. where the color represents the type of surface or feature identified by the model. The result of the classification map of Model 14 is shown in Figure 9. Classification Map Result of Model 14.

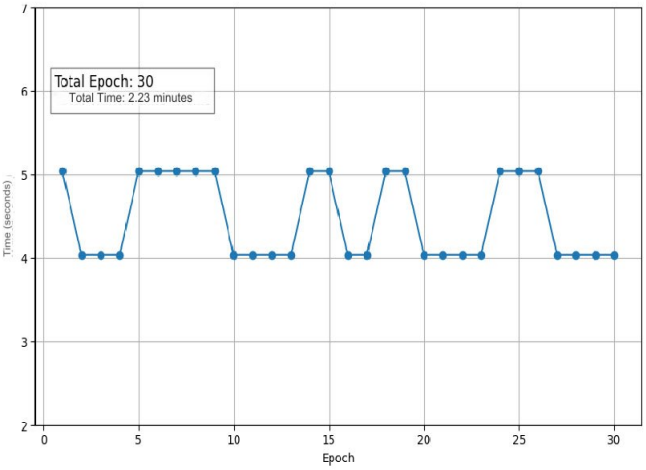

Figure 8. Timestamp Each Epoch of Model 14

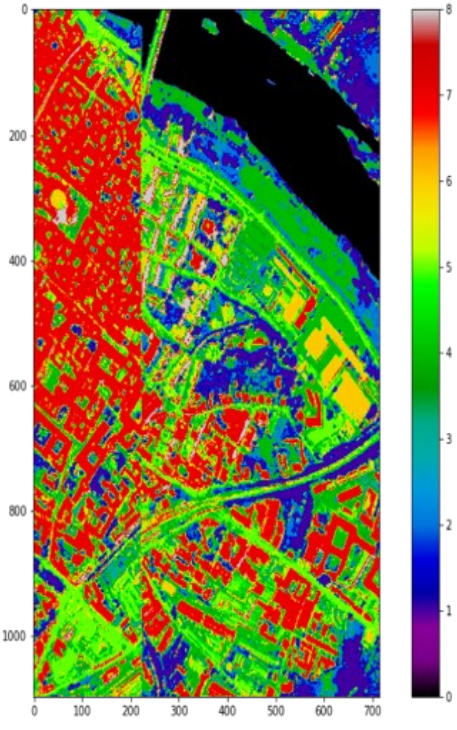

Figure 9. Classification Map Result of Model 14

The classification map of hyperspectral imagery with color representation according to its classification provides a clear overview of the distribution patterns of various material classes within it. The "Water" class. represented by black color. indicates the presence of water with a perfect accuracy level of 100%. The bluish-purple color representing "Trees" reflects areas with vegetation such as trees. with an accuracy level of 99.68%. The "Asphalt" class. indicated by light blue color. indicates hard surfaces like asphalt. with an accuracy of 87.60%. The cyan-blue color representing "Self-Blocking Bricks" refers to buildings with brick materials and an accuracy level of 97.36%. The greenish color representing "Bitumen" denotes materials like bitumen. such as roads. with an accuracy of 97.51%. The yellowish-green color symbolizing "Tiles" depicts roofing or layer materials with an accuracy of 96.45%. The "Shadows" class with orange color represents shadows with an accuracy of 98.90%. The red color representing "Meadows" reflects areas with lush vegetation and an accuracy of 99.98%. while the white color indicating "Bare Soil" shows empty land with the highest accuracy level of 100%.

This classification map helps visualize where each type of material or land cover is located in the image. enabling a deeper assessment of the classification results. There are a total of 9 classes successfully displayed in this classification map image. The use of various color combinations helps clearly distinguish between different material classes. facilitating the identification and interpretation of hyperspectral classification results visually. The color representation used makes it easier to identify and interpret each material class. This greatly aids in visualizing where each type of material or land cover is located within the image. allowing for a more in-depth assessment of the classification results. Additionally. these color visualizations can also aid in comprehension. making the research findings more easily understandable.

B. Comparative Evaluation of Performance Model

Based on the testing conducted on models 1 to 14. the model with the best average accuracy on the Pavia dataset is model 14. which is a combination of Hybrid CNN method and Regularization Technique optimized with Adam Optimizer. Model 14 demonstrates more stable performance compared to the other 13 models. achieving the highest AA and OA accuracies on the Pavia dataset. Model 12. a combination of the 3D CNN method with regularization technique optimized with Adam Optimizer. achieved the second-best performance after model 14 on the Pavia dataset.

TABLE IV. PERFORMANCE COMPARISON

Model	AA	OA
1	89.99%	96.74%
2	90.53%	96.40%
3	91.63%	97.63%
4	92.98%	97.62%
5	92.87%	97.79%
6	94.11%	98.12%
7	92.32%	96.74%
8	95.09%	98.71%
9	94.29%	98.50%
10	95.73%	98.77%
11	92.46%	97.40%
12	97.13%	98.59%
13	94.75%	98.28%
14	97.50%	99.25%

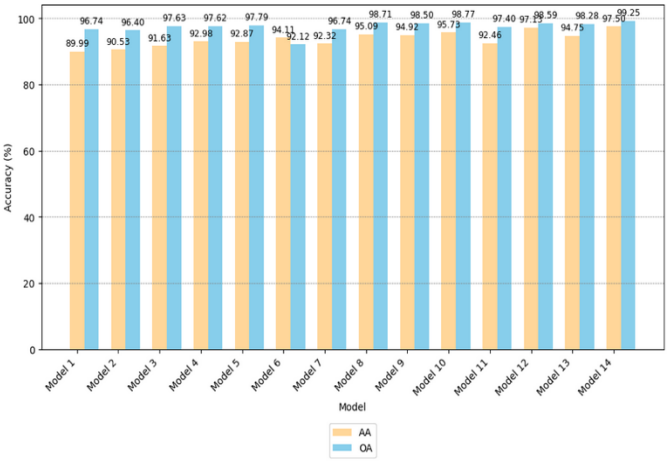

Figure 10. Performance Comparison

The performance comparison of the models is displayed in the following Table IV and Figure 10. The comparison table of model accuracies on the Pavia dataset shows that Model 14 and Model 12 stand out as the models with the highest accuracy. with Average Accuracy (AA) of approximately 97.50% and 97.13%. respectively. and Overall Accuracy (OA) of approximately 99.25% and 98.59%. respectively. This superiority can be attributed to the application of regularization techniques in both models. Model 14 employs a hybrid CNN approach combining CNN features with regularization techniques. while Model 12 uses 3D CNN with regularization. Both models effectively reduce overfitting and enable effective data generalization. especially when additional dimensions are present. such as in video or motion data.

Compared to other studies. these findings are consistent with previous research demonstrating that regularization techniques can significantly enhance CNN model performance in addressing overfitting issues. For instance. showed that using dropout and L2 regularization on CNNs also resulted in improved image classification accuracy [21]. Additionally. emphasized that combining 3D CNNs with regularization techniques can improve model accuracy in the context of temporal and spatial data [22].

However. this study extends the knowledge by showing that the application of regularization to CNN architectures not only improves accuracy in static image data but is also effective in contexts with additional dimensions. such as with hybrid CNN and 3D CNN models with regularization. These findings highlight the importance of tailoring regularization techniques to the type of data being processed and open possibilities for further applications requiring good generalization.

Therefore. this research not only confirms the success of regularization techniques in improving CNN model accuracy but also provides new insights into how these techniques can be optimized for different types of data.

IV. CONCLUSION

This research successfully developed a conventional CNN method with the highest accuracy on the Pavia dataset. with an AA of 97.50% and OA of 99.25% achieved by Model 14. utilizing the Hybrid CNN method and regularization techniques with Adam optimization. The combination of regularization techniques with Adam optimization on the Pavia Center dataset proved to enhance accuracy and classification performance. as evidenced by the comparison of models indicating that regularization techniques and Adam optimization

outperformed by 0.50-1%. The use of Adam optimization and regularization techniques on the Pavia Center dataset effectively addresses classification issues. as demonstrated by more efficient processing time and superior accuracy results. with a computation time of 5.68 minutes achieving an overall accuracy of 99.25%. The limitations of this study include the restricted availability of datasets and the exclusive use of the ADAM optimization method in the developed deep learning model. Future work may explore the application of alternative optimization techniques and the use of more diverse and comprehensive datasets to enhance the model's robustness and generalizability.

REFERENCES

[1] D. Kosasih, M. Buce Saleh, and L. Budi Prasetyo, "Visual and Digital Interpretations for Land Cover Classification in Kuningan District. West Java," *Jurnal Ilmu Pertanian Indonesia*., vol. 24, no. 2, pp. 101–108, Apr. 2019, doi: 10.18343/jipi.24.2.101.

[2] C. Zhao *et al*., "Multiscale construction of bifunctional electrocatalysts for long-lifespan rechargeable zinc–air batteries," *Adv. Funct. Mater.*, vol. 30, no. 36, Sep. 2020, doi: 10.1002/adfm.202003619.

[3] H. J. Kwon, H. I. Koo, and N. I. Cho, "Understanding and explaining convolutional neural networks based on inverse approach," *Cogn. Syst. Res.*, vol. 77, pp. 142–152, Jan. 2023, doi: 10.1016/j.cogsys.2022.10.009.

[4] S. Ghaderizadeh, D. Abbasi-Moghadam, A. Sharifi, N. Zhao, and A. Tariq, "Hyperspectral image classification using a hybrid 3D-2D convolutional neural networks," *IEEE J. Sel. Top. Appl. Earth Obs. Remote Sens.*, vol. 14, pp. 7570–7588, 2021, doi: 10.1109/JSTARS.2021.3099118.

[5] R. Li and X. Ma, "Evaluation and improvement of a CALIPSO-based algorithm for cloud base height in China," *Remote Sens. (Basel)*, vol. 16, no. 15, p. 2801, Jul. 2024, doi: 10.3390/rs16152801.

[6] S. Baamonde, M. Cabana, N. Sillero, M. G. Penedo, H. Naveira, and J. Novo, "Fully automatic multi-temporal land cover classification using Sentinel-2 image data," *Procedia Comput. Sci.*, vol. 159, pp. 650–657, 2019, doi: 10.1016/j.procs.2019.09.220.

[7] L. Qian, L. Hu, L. Zhao, T. Wang, and R. Jiang, "Sequence-dropout block for reducing overfitting problem in image classification," *IEEE Access*, vol. 8, pp. 62830–62840, 2020, doi: 10.1109/ACCESS.2020.2983774.

[8] Y. Zhou *et al*., "Interface-modulated nanocomposites based on polypropylene for high-temperature energy storage," *Energy Storage Mater.*, vol. 28, pp. 255–263, Jun. 2020, doi: 10.1016/j.ensm.2020.03.017.

[9] Y. Liang, B. Dong, P. Li, K. Zhang, and X. Gao, "Prediction of overwintering crane population in Poyang Lake wetland based on RS and regression model, China," *Ecol. Indic.*, vol. 149, p. 110183, May 2023, doi: 10.1016/j.ecolind.2023.110183.

[10] R. Lei *et al*., "Hyperspectral remote sensing image classification using deep convolutional capsule network," *IEEE J. Sel. Top. Appl. Earth Obs. Remote Sens.*, vol. 14, pp. 8297–8315, 2021, doi: 10.1109/JSTARS.2021.3101511.

[11] H. Pan, X. Zhao, H. Ge, M. Liu, and C. Shi, "Hyperspectral image classification based on multiscale hybrid networks and attention mechanisms," *Remote Sens. (Basel)*, vol. 15, no. 11, p. 2720, May 2023, doi: 10.3390/rs15112720.

[12] C. Pu, H. Huang, and L. Yang, "An attention-driven convolutional neural network-based multi-level spectral–spatial feature learning for hyperspectral image classification," *Expert Syst. Appl.*, vol. 185, p. 115663, Dec. 2021, doi: 10.1016/j.eswa.2021.115663.

[13] X. Luo, X. Tong, Z. Hu, and G. Wu, "Improving urban land cover/use mapping by integrating a hybrid convolutional neural network and an automatic training sample expanding strategy," *Remote Sens. (Basel)*, vol. 12, no. 14, p. 2292, Jul. 2020, doi: 10.3390/rs12142292.

[14] M. Kavitha, *et al*., "Performance evaluation of deep e-CNN with integrated spatial-spectral features in hyperspectral image classification," *Measurement*, vol. 191, p. 110760, Mar. 2022, doi: 10.1016/j.measurement.2022.110760.

[15] B. Xie, H. K. Zhang, and J. Xue, "Deep convolutional neural network for mapping smallholder agriculture using high spatial resolution satellite image," *Sensors*, vol. 19, no. 10, p. 2398, May 2019, doi: 10.3390/s19102398.

[16] M. Ahmad, M. Mazzara, and S. Distefano, "Regularized CNN feature hierarchy for hyperspectral image classification," *Remote Sens. (Basel)*, vol. 13, no. 12, p. 2275, Jun. 2021, doi: 10.3390/rs13122275.

[17] M. Ahmad, A. M. Khan, M. Mazzara, S. Distefano, S. K. Roy, and X. Wu, "Hybrid dense network with attention mechanism for hyperspectral image classification," *IEEE J. Sel. Top. Appl. Earth Obs. Remote Sens.*, vol. 15, pp. 3948–3957, 2022, doi: 10.1109/JSTARS.2022.3171586.

[18] A. Mohan and M. Venkatesan, "HybridCNN based hyperspectral image classification using multiscale spatiospectral features," *Infrared Phys. Technol.*, vol. 108, p. 103326, Aug. 2020, doi: 10.1016/j.infrared.2020.103326.

[19] W. H. Lopez Pinaya, S. Vieira, R. Garcia-Dias, and A. Mechelli, "Convolutional neural networks," in *Machine Learning*, Elsevier, 2020, pp. 173–191, doi: 10.1016/B978-0-12-815739-8.00010-9.

[20] M. E. Paoletti and J. M. Haut, "Adaptable convolutional network for hyperspectral image classification," *Remote Sens. (Basel)*, vol. 13, no. 18, p. 3637, Sep. 2021, doi: 10.3390/rs13183637.

[21] J. Li, B. Liang, and Y. Wang, "A hybrid neural network for hyperspectral image classification," *Remote Sens. Lett.*, vol. 11, no. 1, pp. 96–105, Jan. 2020, doi: 10.1080/2150704X.2019.1686780.

[22] G. Yao, T. Lei, and J. Zhong, "A review of convolutional-neural network-based action recognition," *Pattern Recognit. Lett.*, vol. 118, pp. 14–22, Feb. 2019, doi: 10.1016/j.patrec.2018.05.018.